4. Intraparticle Diffusion*

In the hydrogenation of edible fats and oils over porous nickel catalysts, intraparticle mass transfer limitations not only reduce catalyst effectivities, but also may change the product selectivities. Information from open literature on the possible role of intraparticle diffusion limitation in oil hydrogenation is very limited however. In line with literature we have measured the intraparticle effective diffusion coefficient D_e of edible oils, their fatty acid methyl esters, and of hydrogen under both inert and reaction conditions. The intrinsic kinetic rate equations of Chapter 2 were applied to calculate D_e from hydrogenation experiments (reaction conditions). Comparison with D_e obtained from tracer pulse column experiments (inert conditions) have led to new insights on the pore structure of the catalyst. Besides, this chapter reports on the experimental and mathematical aspects of both experimental methods.

* This chapter is published as "Intraparticle diffusion limitation in the hydrogenation of monounsaturated oils and their fatty acid methyl esters", Jonker, G. H.; Veldsink, J. W.; Beenackers, A. A. C. M.; *Ind. Eng. Chem. Res.*, **1998**, *37*, 4646-4656.

4.1. Introduction

Coenen (1986) has summarized the data on diffusion limitation in hydrogenation of edible oils and reported for a narrow pore catalyst (mean pore diameter $<d_c>$ ≈ 4 nm) a 50% decrease in activity relative to a medium- ($<d_c>$ ≈ 6 nm) and wide-pore ($<d_c>$ ≈ 8 nm) catalyst. Colen et al. (1988) have observed intraparticle diffusion limitation in trioleate hydrogenation from which they have calculated intraparticle TAG diffusion coefficients of $D_{e,TAG} = 2 \times 10^{-11}$ m²/s (wide-pore catalysts) and 4×10^{-12} m²/s (medium-pore catalysts) (T = 373 K) and an absence of hydrogen limitation. For methyl ester hydrogenation over Pd/C catalysts, Tsuto et al. (1978) could verify the observed shunt reactions by incorporating intraparticle hydrogen diffusion limitation, though not very accurately, because of the insensitivity of the curves for the value of D_e. We are not aware of any other data, which is surprising in light of the substantial effects intraparticle diffusion limitation may have on the selectivity of the reaction.

Effective intraparticle diffusion coefficients D_e are usually estimated from the bulk liquid coefficients D_b by calculating a factor for hindered diffusion which is commonly taken as (Satterfield et al., 1973):

$$D_e = 10^{-2l} \frac{e_p}{t} D_b \tag{4.1}$$

$$l = \frac{d_m}{< d_c >} \tag{4.2}$$

The empirical eq 4.1 was tested in the range of $0.1 < l < 0.5$ (Satterfield et al., 1973). There is a lack of data concerning the change of steric hindrance inside catalyst pores with varying degrees of unsaturation (Veldsink et al., 1997), although the oil's viscosity and the bulk coefficient remain unchanged (Veldsink et al., 1997). For TAGs, D_b has been measured by Andersson et al. (1974), but because of the uncertainties in the values of $<d_c>$ and t, only rough estimates are available for D_e in edible oil hydrogenation over porous catalysts (Veldsink et al., 1997).

Preferably, D_e should be determined under reaction conditions, but this requires a thorough knowledge of the intrinsic kinetics. Additional data on D_e can be obtained from independent experiments in the absence of reaction (Haynes, 1988). In line with the recommendations in the literature (Park and Kim, 1984; García-Ochoa and Santos,

1994), we have measured D_e both under inert and reaction conditions. However, for catalyst particles with nonuniform pores, a difference of one order of magnitude or more can be expected between the measured values of D_e in both types of experiments (Park and Kim, 1984; García-Ochoa and Santos, 1994), which is well documented for reactions in zeolites (Chen et al., 1994).

McGreavy et al. (1994) showed the large influence of the pore structure on the value of D_e, in terms of micro- and macropores and their connectivity. Among others, Park and Kim (1984) and García-Ochoa and Santos (1994) investigated the reaction and diffusion in bimodal-supported catalysts, which were modelled as pellets and assembled as crystallites. For this macro- and micropore system, they found D_e under nonreaction conditions to vary from 2 to 20 times larger than D_e measured under reaction conditions. Although the exact reasons for these differences are not fully understood, the contributions of the pore structure to the value of D_e can be expected to vary with the experimental technique (Park and Kim, 1984; García-Ochoa and Santos, 1994).

For an independent determination of D_e, i.e., without using reaction data, the HPLC (high performance liquid chromatography) method is the most suited technique (Haynes, 1988). Nevertheless, for small non-zeolite catalyst particles, such tracer pulse experiments have been rarely performed for the determination of the effective liquid pore diffusion coefficients (Ma and Lin, 1987; Lin and Ma, 1989; Hejtmánek and Schneider, 1994). The main reasons are the occurrence of instabilities in column packing due to the small particle sizes ($d_p < 10$ *m*m) (Cumberland and Crawford, 1987) and, with respect to the catalyst strength, intolerable high pressure drops over the column (Lin and Ma, 1989). Moreover, the accuracy of obtaining D_e is lower for small particles, since diffusion and mass-transfer times become comparable to dispersion times (Hejtmánek and Schneider, 1994). An exception are zeolites where D_e is low enough to completely determine trace pulse dispersion ($D_e \approx 2 \times 10^{-12}$ m^2/s). Therefore, most HPLC results on diffusivity were obtained for zeolites, while data on small non-zeolite particles are scarce (Ma and Lin, 1987).

We have studied the intraparticle liquid diffusion coefficients of FAME, TAG, and hydrogen for small nickel-on-silica catalysts under reaction conditions and by applying tracer pulse column experiments in the absence of the hydrogenation reaction. For studying D_e under reaction conditions, we derived the true intrinsic hydrogenation kinetics from a wide range of hydrogenation experiments in the absence of diffusion limitation (see Chapter 2). These rate equations are used here to

investigate the effects of intraparticle hydrogen and FAME or TAG diffusion on the hydrogenation rate. Also, by applying recent improvements in column-packing techniques and realizing various improvements in experimental accuracy, we now can report the first data on effective intraparticle liquid diffusion coefficients of FAME and TAG in porous non-zeolite nickel-on-silica catalysts from HPLC experiments in the absence of hydrogenation. The D_e values obtained from these two methods will be compared.

4.2. Theory

4.2.1. D_e from the Reaction Data. The intrinsic kinetic rate equations of the conversion rate of methyl oleate (methyl ester of oleic acid, O) and methyl elaidate (E) were taken from Chapter 2. The experimentally determined rate equations are

$$R_O = m_c \frac{-(k_1(T) + k_2(T)K_{iso})C_O + k_2(T)C_E}{C_O + C_E + k_4(T)C_S} K_H P_{H_2} \qquad (4.3)$$

$$R_E = m_c \frac{-(k_3(T) + k_2(T))C_E + k_2(T)K_{iso}C_O}{C_O + C_E + k_4(T)C_S} K_H P_{H_2} \qquad (4.4)$$

The adjusted parameters (k_i) depend on the temperature (T [K]) according to an Arrhenius relation:

$$k_i(T) = k_{i,ref} \exp\left(\frac{-E_{a,i}}{R_{gas}T_{ref}}\left(\frac{T_{ref} - T}{T}\right)\right) \qquad (4.5)$$

The parameters are given in Table 4.1 for Pricat 9910 (sample 1992, Unichema, Emmerich).

Additional batch hydrogenations were performed to obtain D_e under diffusion-controlled conditions. The coupling of mass transport and intrinsic kinetic rate constants is described by the particle mass balance, which reads (Westerterp et al., 1987)

$$D_{e,i}\frac{\partial}{\partial r_p}\left[r_p^2\frac{\partial C_i}{\partial r_p}\right]=R_{V,i}r_p^2 \qquad i=\mathrm{O,\ E,\ H_2} \tag{4.6}$$

Here $R_{V,i}$ is the local volumetric reaction rate. Boundary conditions are

$$\left(\frac{\partial C_{s,i}(t,r_p)}{\partial r_p}\right)_{r_p=0}=0$$

$$C_{s,i}(t,R_p)=C_{b,i}(t)$$

$$C_{b,i}(0)=C_{b,i}^0 \tag{4.7}$$

Table 4.1. Reaction Rate Constants with 95% Confidence Limits (Chapter 2) [a].

compound parameter	value at T_{ref}	E_a [kJ/mol]
k_1	4.14 ± 0.14 [b]	32.2 ± 0.7
k_2	1.54 ± 0.15 [b]	47.2 ± 4.2
k_3	3.94 ± 0.32 [b]	28.1 ± 3.1
k_4	0.32 ± 0.04 [c]	

[a] K_{iso} = 3.5 (Litchfield et al., 1963); DH_{iso} = –4 kJ/mol (Rogers et al., 1974); T_{ref} = 393 K. [b] units: [kg_l/kg_{Ni} MPa s]. [c] dimension: none.

Preliminary calculations showed that the external particle mass-transfer resistance typically is 5% for the average particle diameter (up to 10% for the largest particles) of the total resistance only. This is a normal value for batch hydrogenations of edible oils in laboratory-scale reactors (Bern et al., 1975; Cordova and Harriot, 1975; Gut et al., 1979). The hydrogen uptake equals the sum of the O and E reaction rate:

$$R_{H_2}=\frac{dC_{b,S}}{dt}=-\sum_i\frac{dC_{b,i}}{dt} \qquad i=\mathrm{O,\ E} \tag{4.8}$$

The differential equations (4.6) were solved numerically. The time scale for concentration changes in the bulk liquid is long relative to that in the catalyst particles (Colen et al., 1988), which leads to pseudosteady states with a constant C_b within one

time interval (Colen et al., 1988). Time integration of the bulk concentration change was performed using a fifth-order Runga–Kutta method with an adaptive step size. The experimental curves were used to obtain a value for the unknown parameter D_e by fitting the model curves.

The differential equations were solved with estimated values for the intraparticle effective diffusion coefficients, D_e, and using the intrinsic kinetic rate constants of Table 4.1. The deviations of the resulting model calculations for an estimated D_e were subsequently used to calculate a c^2-target function for $N_{e,d}$ experimental points of the N_e experiments with $N_{e,i}$ components:

$$c^2 = \frac{1}{N_e} \sum_{e=1}^{N_e} \frac{1}{N_{e,i} N_{e,d}} \sum_{i=1}^{N_{e,i}} \sum_{e=1}^{N_{e,d}} \frac{(C^e_{e,i,d} - C^m_{e,i,d})^2}{s^2_{i,d}} \tag{4.9}$$

The Levenberg–Marquardt algorithm (Press et al., 1987) was then used to optimize D_e. To compare various the experimental series, the total variance was used:

$$S^2 = \frac{\sum_{e=1}^{N_e} \sum_{i=1}^{N_{e,i}} \sum_{d=1}^{N_{e,d}} (C^e_{e,i,d} - C^m_{e,i,d})^2}{\sum_{e=1}^{N_e} ((N_{e,d} - 1) N_{e,i}) - N_{fit}} \tag{4.10}$$

with N_{fit} being the number of optimized parameters.

Finally, an overall efficiency of the catalyst for a component i, m_i, can be calculated from the ratio of the actual reaction rate ($J_i a_s$) and the maximum possible reaction rate, based on bulk liquid concentrations, $R_i(C_i)$ (Westerterp et al., 1987):

$$m_i = \frac{J_i a_c}{R_i(C_i)} \qquad i = \mathrm{O},\ \mathrm{E},\ \mathrm{H_2} \tag{4.11}$$

$m_i < 0.95$ indicates significant diffusion limitation, whereas $m_i > 0.95$ indicates neither intraparticle TAG or FAME nor hydrogen limitation.

From the experimental curves, D_e was obtained for intraparticle diffusion-limited hydrogenation runs of both FAMEs and TAGs. The confidence intervals of optimized D_e were determined using the maximum and minimum possible values of the conversion rates of O and E at the surface according to the 95% confidence limits of the intrinsic kinetic rate constants given in Table 4.1.

4.2.2. D_e from HPLC data. For the mathematical modeling of tracer pulse injection in packed columns we followed the method of Hejtmánek and Schneider (1994). The key parameters in their time domain simulation of the RTD curve are the Peclet number, Pe_{ax}, the effective intraparticle diffusion coefficient, D_e, and the retention volume V_r.

The Peclet or the Bodenstein number reflects the axial dispersion in the column packing:

$$Bo = \frac{d_p v}{D_{ax}} \qquad Pe_{ax} = \frac{Lv}{D_{ax}} \tag{4.12}$$

In the laminar flow regime (which always holds for HPLC) theoretically Bo = 0.5 (Westerterp et al., 1987).

The transport inside the particles is described by a Fickian diffusion equation in which the pore hindrance is accounted for by the effective diffusion coefficient. Although for $l \rightarrow 1$ (micropores) surface diffusion of adsorbed species should be incorporated, the adsorption on the pore wall is negligible in this study, so D_e can be applied to both the macro- and the micropore regimes (Lin and Ma, 1989). The external particle mass transfer was neglected (Lin and Ma, 1989). The validity of this assumption was justified afterwards by incorporating the external particle mass-transfer into the mass balances and using Sh (= $k_s d_p/D_b$) = 4 (Bern et al., 1975) and the experimentally determined D_e.

V_r follows for linear adsorption (represented by K_s, after Hejtmánek and Schneider, 1994) from Φ_v and MO1:

$$V_r \equiv \Phi_v \mathrm{MO1} = (e_b + (1 - e_b) e_p (1 + K_s)) V_{cl} \tag{4.13}$$

MO1 is the first moment of the RTD curve (Westerterp et al., 1987)

$$\mathrm{MO1} = q_{\mathrm{m}} t = t \int_0^\infty qE(q)\mathrm{d}q \qquad (4.14)$$

With eq 4.13, V_r can be calculated from the first moment of the RTD curve (4.14), which served as a start value in the optimization procedure.

Parameters D_e and Pe_{ax} and the final value of V_r were obtained from a best fit of the time domain solution of Hejtmánek and Schneider (1994) to the experimental elution curves by using the Levenberg–Marquardt algorithm (Press et al., 1987) and c^2, defined by eq 4.9. The parameter optimization procedure was adjusted to obtain the most accurate values, using a wide range of experimental RTDs simultaneously.

4.3. Experimental Section

4.3.1. Hydrogenation Experiments. The hydrogenation of FAME was carried out in a 600-mL agitated, dead-end autoclave. To avoid induction effects, the catalyst was regenerated in situ at P_{H_2} = 0.5 MPa and T = 473 K for 2 h, followed by evacuation for 0.5 h prior to the hydrogenation. The reactor is described in Chapter 2. The autoclave was well stirred (25 rps, with baffles, volumetric gas–liquid mass transfer determined at high catalysts loads, $k_l a$ = 1.8 s^{-1}, see Chapter 2), and the temperature was controlled within 1 K. Another, smaller (300 mL) but otherwise similar, reactor was used too, for which $k_l a$ was measured independently as $k_l a$ = 0.8 s^{-1} (see Chapter 3). The liquid-phase composition (O, E, S) was measured by gas chromatography (Hewlett Packard 5890) with a Chrompack CP-sil 88 column. The autoclaves were operated at constant hydrogen pressure, and during the course of the reaction, 15 samples were taken from the reaction mixture and analyzed afterwards.

Table 4.2 lists the diffusion-limited FAME and TAG experiments with Pricat 9910 (sample 1992; Unichema, Emmerich). The pore size distribution of Pricat 9910 is given in Figure 4.1, both from nitrogen adsorption isotherm data (Figure 4.1A, covering pore size ranges from 1 to 30 nm) and from mercury porosimetry (Figure 4.1B, accurate in the 7-nm to 10-*m*m range (Le Page et al., 1987)). The overall conversion rates were kept below 10% of the hydrogen gas–liquid mass transfer rate by adjusting the catalyst load. The FAME experiments were carried out at T = 443 K, because at lower temperatures intraparticle diffusion limitation appeared to be absent (see Chapter 2). The TAG experiments (sunflower oil and trioleate) were performed in the temperature range 373 < T < 443 K and 0.30 < P_{H_2} < 0.50 MPa (see Table 4.2).

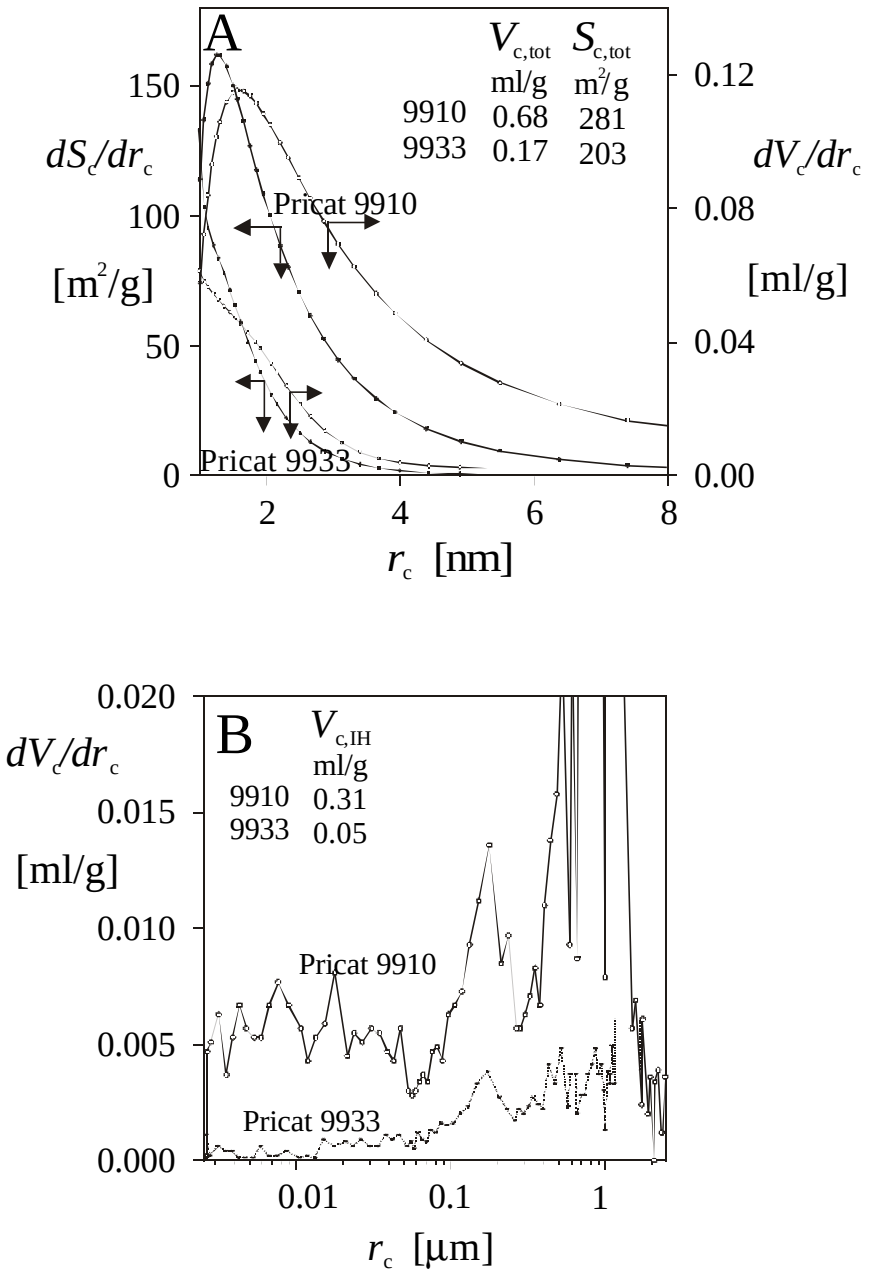

Figure 4.1. Pore surface and volume of Pricat 9910 (sample 1992) and Pricat 9933 (sample 1992). (A) Differential specific pore surface (left axis) and pore volume (right axis) plot; data from BET measurements. (B) Specific pore volume measured by mercury porosimetry. Subscripts tot and IH are "total" and "intercrystalline" holes, respectively.

Table 4.2. Diffusion-Limited Hydrogenation Experiments.

expno	source	P_{H_2} MPa	T, K	h [a] 10^{-3} Pa s	m_{H_2} [b] m^3_g/m^3_l	C_O^0/C_{tot}	C_E^0/C_{tot}	C_S^0/C_{tot}
1	FAME	0.02	443	0.3	0.15	0.445	0.306	0.249
2	FAME	0.08	443	0.3	0.15	0.275	0.497	0.228
3	FAME	0.08	443	0.3	0.15	0.723	0.182	0.095
4	FAME	0.50	443	0.3	0.15	0.448	0.314	0.238
5	TAG	0.30	403	4	0.09	0.139	0.074	0.787
6	TAG	0.30	443	2	0.12	0.122	0.092	0.786
7	TAG	0.50	373	10	0.07	0.104	0.056	0.840
8	TAG	0.50	443	2	0.12	0.097	0.073	0.830
9	TAG	0.50	443	2	0.12	0.268	0.321	0.411

[a] TAG-data: Eiteman and Goodrum, 1994; FAME data from internal data. [b] Veldsink et al., 1997.

4.3.2. HPLC Experiments. The setup consisted of a column (L = 0.05 or 0.10 m, $d_{cl} = 4.6 \times 10^{-3}$ m) packed with Pricat 9933, an HPLC pump (Bromma–LKB 2150), injector (Valco), and an on-line differential refractory index meter (Waters Millipore

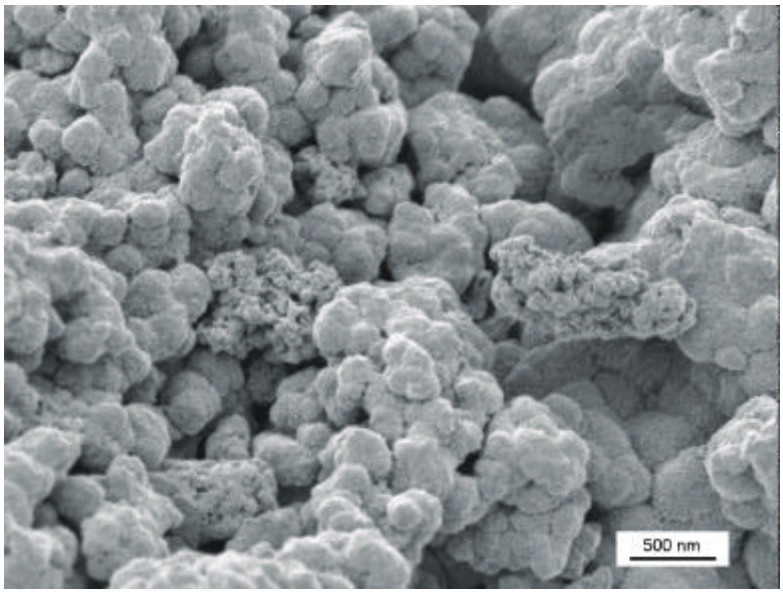

Figure 4.2. Electron microscope picture of Pricat 9933, representative for Pricat 9910 too.

410). Eluents were degassed, filtered, and stored under nitrogen. A tracer (1–10 mol %) was injected in an amount of 0.02% of the column volume. The linearity of the detection cell was examined by varying the injection sample concentration (Lin and Ma, 1989). The flow was determined by weighing the eluted liquid.

Pricat 9933 (from Unichema, Emmerich) was used, which resembles generally applied hydrogenation catalysts (nickel-on-silica carrier, e.g., Pricat 9910), but with a

Table 4.3. Experimental Series. [a]

col	L, m	eluent	formula	M, kg/mol	η, mPa s	$10^{10}\Phi_v$, m^3/s	$10^{-3}\rho_l$, kg/m^3	T K
C1	0.05	*n*-octane	C_8H_{18}	0.114	0.45[b]	8–80	0.681[b]	298–35
C2	0.10	MCT oil[c]	$C_{30}H_{59}O_6$	0.515	17[d]	3–10	0.930[d]	313–35

[a] $d_{col} = 4.6 \times 10^{-3}$ m; $d_p = 10^{-5}$ m. [b] Handbook, $T = 313$ K. [c] Supplied by van den Berg & Jurgens, The Netherlands. [d] $T = 313$ K, internal data.

Table 4.4. The Tracers

tracer	formula	code	M_w kg/mol	d_m nm	l[a]	$10^{-2}l$ (eq 5.1)	N_{DI}
n-hexadecane	$C_{16}H_{34}$	HD	0.226	0.5[b]	0.13	0.55	0
methyl palmitate	$C_{17}H_{34}O_2$	MP	0.272	0.8[c]	0.20	0.40	0
trioleate	$C_{57}H_{104}O_6$	TO	0.888	1.0[d]–2.0[e]	0.25–0.50	0.32–0.10	3
soy bean oil[f]	$C_{57}H_{100}O_6$	SB	0.884	1.0[d]–2.0[e]	0.25–0.50	0.32–0.10	5
cholesterol	$C_{28}H_{48}O$	CH	0.386	1.3[c]	0.33	0.22	1

[a] $\langle d_c \rangle = 4$ nm. [b] Satterfield et al., 1973; Chen et al., 1994. [c] Chen et al., 1994. [d] Lowest reported value: Bern et al., 1975. [e] highest reported value: Coenen, 1986. [f] mixture of fats with unsaturation varying from 4 to 6, average: 5.

low mean pore size ($\langle d_c \rangle = 4$ nm, "narrow-pores" according to Coenen (1986)) with the smallest possible pore-size distribution. However, an electron microscopy photograph (Figure 4.2) shows that the particles are built from sintered crystallites giving rise to large, inter crystalline, pores. The pore size distribution shows the larger pores as a peak around 0.5 *m*m in Figure 4.1B.

It is very difficult to obtain a uniform column packing with small particles. The packing is improved by a uniform particle size (Cumberland and Crawford, 1987). Pricat 9933 was freed from fines with the "sludge" method, yielding a narrow (volume) particle-size distribution curve (for details, see Jonker et al., 1997). The technology of Chrompack was used to get columns with a good plug-flow behavior.

Eluent and column features are summarized in Table 4.3, for data on tracers applied, see Table 4.4. Column degeneration was checked after each ten experiments by repetition of a "standard" experiment, being 5 mol% hexadecane in either *n*-octane (column C1) or MCT oil (column C2), with $\Phi_v = 4 \times 10^{-9}$ m^3/s. Both columns appeared to remain stable.

4.4. Results

4.4.1. Simulation of H_2 or FAME/TAG Diffusion Limitation during Reaction.

The qualitative effect of either hydrogen or FAME/TAG intraparticle diffusion limitations on the reactant and product conversion curves can be investigated by solving the model (eqs 3–7) with the parameters from Table 4.1 for various values of D_e. Figure 4.3 gives intraparticle concentration profiles of O, E and S at t = 0 for experiment 3 (Table 4.2) for m_{H_2} = 0.25, in case intraparticle transport of FAME is limited by diffusion limitation ($D_{e,FAME}$ = 1.25 × 10^{-13} m^2/s, $D_{e,H_2} \rightarrow \infty$. The different

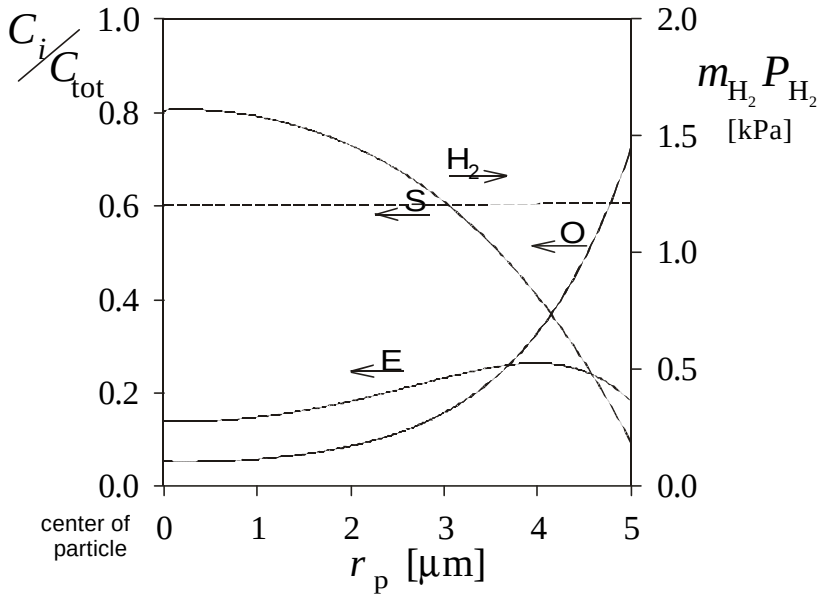

Figure 4.3. Typical initial catalyst concentration profile for experiment 3, Table 4.2, m_{H_2} = 0.25. Fame diffusion limitation ($D_{e,FAME}$ = 1.25 × 10^{-13} m^2/s). Solid lines, FAME (O, E, S); dotted line, H_2. Model equations, eqs 4.3 and 4.4; k values, Table 4.1.

intraparticle concentration profiles will result in different relative rates of hydrogenation of the *cis* and *trans* isomers. Figure 4.4 shows the fraction of O and E as a function of the double bond conversion (z_{DB} [%]) for diffusion limitation of both FAME only and of hydrogen only. Compared to the kinetically limited regime, FAME diffusion limitation changes the reactant distribution curves considerably, whereas hydrogen diffusion limitation does not affect the reaction curves. Therefore, the relative formation of *trans* isomers reveals information on which type of diffusion limitation occurs.

In the case of FAME/TAG limitation, there is an increasing chance of an already isomerized molecule to be hydrogenated before leaving the catalyst (Van der Plank, 1972b). As a result, the amount of E will be reduced at elevated temperatures. Owing to the preferred formation of E at higher T, both thermodynamically and kinetically,

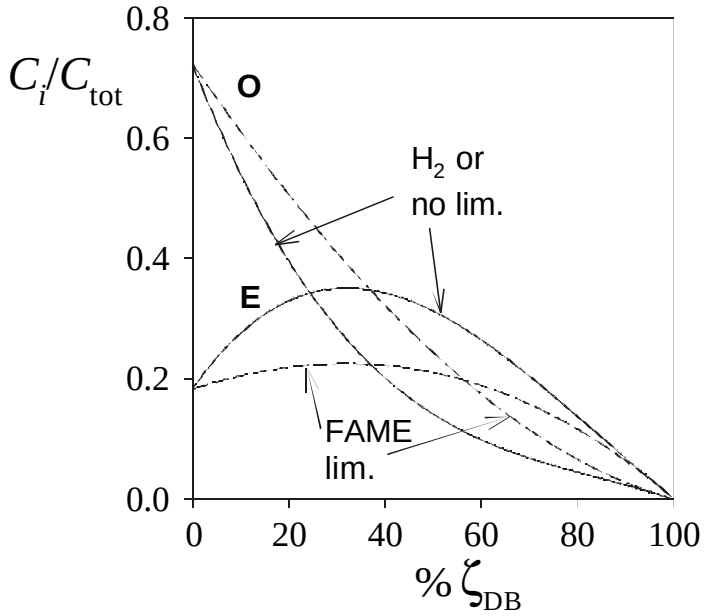

Figure 4.4. Influence of H_2 and FAME/TAG limitation in a conversion plot (fractions of O and E as a function of fraction S) for an initially similar catalyst efficiency of experiment 3, Table 4.2. Solid lines, model lines without diffusion limitation ('no lim'); dotted lines, H_2 limitation ('H_2 lim') ($D_{H_2} = 1.5 \times 10^{-10}$ m^2/s, $m_{H_2} = 0.25$); dashed lines, FAME limitation ('FAME lim.'; $D_{e,FAME}$ or $D_{e,TAG} = 1.25 \times 10^{-13}$ m^2/s, $m_{H_2} = 0.25$). Model equations, eqs 4.3 and 4.4; k values, Table 4.1.

the influence of FAME limitation is much lower for an initially E-rich mixture.

4.4.2. Evaluation of D_e from FAME Hydrogenations. To fit H_2 and FAME diffusion coefficients, the experiments at T = 443 K, 0.02 ≤ P_{H_2} ≤ 0.50 MPa (Table 4.2, experiments 1–4) were used simultaneously. Other parameters were set at a fixed value (Table 4.5). The optimization procedure was as follows: (1) determine c^2 at T = 443 K, without applying diffusion limitation; (2) fit of D_{e,H_2} by minimization of c^2 (eq 4.9) with presupposed absence of FAME limitation; (3) fit of $D_{e,FAME}$ by minimization of c^2 (eq 4.9) with a presupposed absence of H_2 limitation; (4) use values of 2 and 3 to start the final optimization of both D_{e,H_2} and $D_{e,FAME}$. The resulting values for the most optimal D_e and the variances (eq 4.10) are listed in Table 4.6. Figure 4.5 plots the residuals.

Both Figure 4.5 and Table 4.6 show that assuming H_2 limitation improves the fits considerably, relative to assuming FAME limitation. The low impact of FAME on the fit also follows from the calculated ratio of $D_{e,FAME}C_{FAME}/D_{e,H_2}C_{H_2} > 10^4$ from the optimized parameters in the final optimization. The two encircled areas in Fig. 5 give the residuals of the S and E fraction if FAME diffusion limitation is applied. The smallest residuals are obtained if H_2 limitation is applied (full symbols). The optimum diffusion coefficient for hydrogen appears to be $D_{e,H_2} = 1.6 \pm 0.7 \times 10^{-10}$ m^2/s. From the appropriate mass balances and using the parameters of Table 4.5, it appeared that the external particle mass-transfer limitation was negligible. This is confirmed by the Biot number ($Bi = k_s d_p/D_e$): $Bi > 10^2$. There is a marked influence of H_2 diffusion limitation.

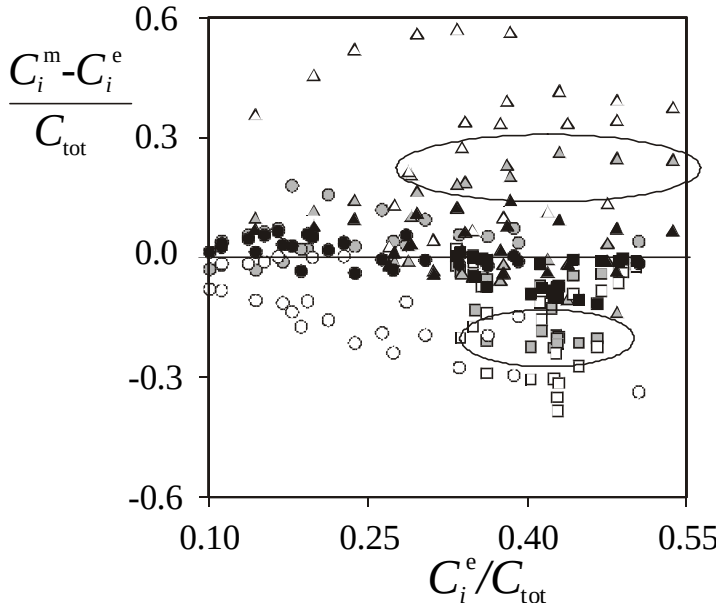

Figure 4.5. Residuals plot of FAME experiments of Table 4.2. Model predictions assuming no diffusion limitation, open symbols; model extension with intraparticle FAME diffusion limitation, gray symbols, and of H_2, black symbols. ● = total of O; ■ = total of E; s = total of S. Model equations, eqs 4.3 and 4.4; *k* values, Table 4.1.

4.4.3. Evaluation of D_e from TAG Hydrogenations. The TAG hydrogenations were also evaluated on TAG and/or H_2 intraparticle mass-transfer limitation. The hydrogenations were performed with polyunsaturated sunflower oils, but to evaluate the intraparticle diffusion coefficient, we used the monoenic part of the hydrogenation curves only. In these simulations, two extra assumptions had to be made: (1) The kinetics of double bonds in TAG are to be taken equal to those of FAME, as there are

no experimental data (Veldsink et al., 1997; Van der Plank et al., 1972b). Therefore, Table 4.1 is also valid for TAG. (2) All three fatty acids in the triacylglycerol are equally reactive to hydrogenation and to isomerization (Tumer et al., 1964).

Table 4.5. Parameter Values Used in the Optimizations

param	value	dimen	comments
d_p	8.4	mm	Coulter Counter Multisizer II
r_c	1.2×10^3	kg_c/m^3_c	own density measurements (gaseous)
m_{Ni}	0.66	kg_{Ni}/kg_c	
r_l	762	kg_l/m^3_l	own density measurements (T = 443 K)
T	443	K	
D_{H_2}	2×10^{-8}	m^2/s	Andersson et al., 1974; T = 443 K
$D_{b,TAG}$	3×10^{-10}	m^2/s	Andersson et al., 1974; T = 443 K
Sh	4	-	Bern et al. 1975
C_{tot}	2.5×10^3	mol/m^3	T = 443 K

Table 4.6. Effective Diffusion Coefficients from FAME and TAG Hydrogenation Experiments at T=443 K

exp. series→		FAME		TAG	
case	limitation	S^2	optimal D_e	10^3*S^2	optimal D_e
1	any	0.0342		1.411	
2	H_2	0.0028	$(1.6 \pm 0.6) \times 10^{-10}$	0.102	*a*
3	oil	0.0129	*a*	0.039	$(3.3 \pm 1.1) \times 10^{-12}$
4	H_2 and oil	0.0029	*b*	0.012	*c*
main diff. lim. →		H_2		TAG	

[a] high value of S^2, due to nonoptimal fit. [b] Ratio $D_{e,FAME}C_{FAME}/D_{e,H2}C_{H2}$ > 10, implying complete hydrogen limitation. [c] $D_{e,H2}$ and $D_{e,TAG}$ highly correlated; $D_{e,H2}$ not significant (see text)

The optimization strategy was the same as for FAME. Table 4.6 shows the results of fitting both D_{H_2} as well as $D_{e,TAG}$ for experiments at T = 443 K. Here, assuming H_2 limitation gives a small improvement (10^3S^2 = 0.012) relative to assuming no diffusion limitation (10^3S^2 = 0.039), see Table 4.6. Also for TAG hydrogenation, $Bi > 10^2$. For the ratio $D_{e,TAG}C_{TAG}/D_{H_2}C_{H_2}$ a value of around 0.5 was calculated, which indicates comparable hydrogen and TAG limitation. However, in section 4.4.1, it was demonstrated that hydrogen limitation or TAG/FAME limitation each has a marked influence on the reaction curves. Model curves assuming hydrogen limitation predict a much higher *trans* formation than is actually observed in TAG hydrogenation (see

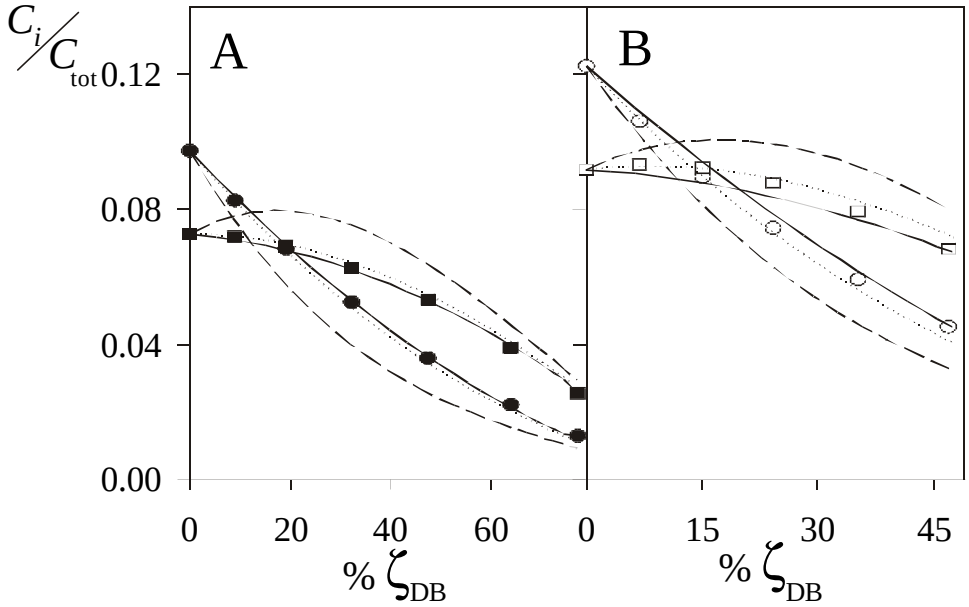

Figure 4.6. Diffusion limitation in TAG hydrogenation experiments. (A) 443 K, 0.50 MPa (experiment 8, Table 4.2). (B) 443 K, 0.30 MPa (experiment 6, Table 4.2). Solid lines, TAG limitation ($D_{e,TAG} = 3.3 \times 10^{-12}$ m^2/s); dashed lines, absence of diffusion limitation or H_2 limitation; dotted lines, both TAG and H_2 limitation. ● = total of O; ■ = total of E. Model equations, eqs 4.3 and 4.4; *k* values, Table 4.1.

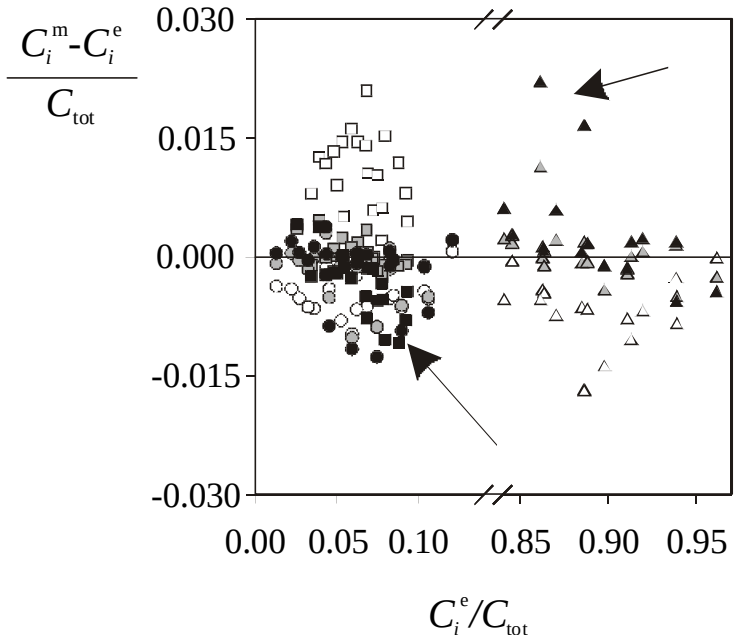

Figure 4.7. Residuals plot of TAG experiments of Table 4.2. Model assuming intraparticle hydrogen diffusion limitation, open symbols; assuming TAG diffusion limitation, gray symbols; model allowing for both H_2 and TAG diffusion limitation, black symbols. ● = total of O; ■ = total of E; s = total of S. Model equations, eqs. 4.3 and 4.4; *k* values, Table 4.1.

Figure 4.6), while incorporation of TAG diffusion limitation appear to follow

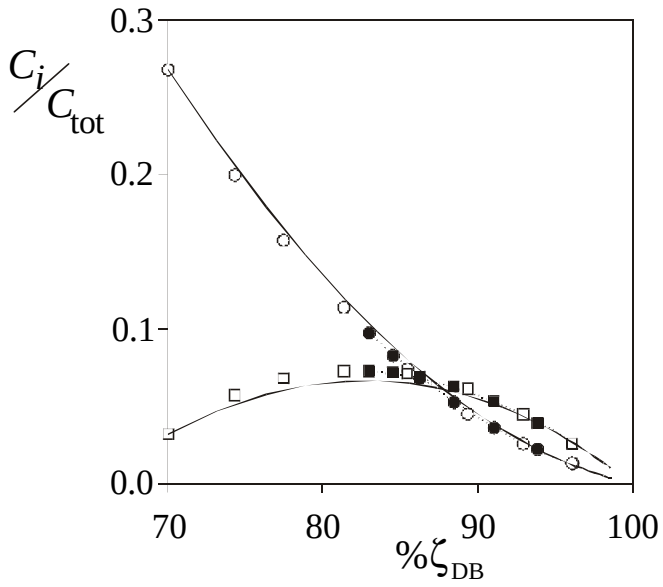

Figure 4.8. Data of synthetic trioleate hydrogenation (experiment 9 of Table 4.2) in the conversion domain, compared to model prediction from sunflower hydrogenation. Sunflower oil: ● = total of O; ■ = total of E. Trioleate: ○ = total of O, □ = total of E. Lines, $D_{e,TAG} = 3.3 \times 10^{-12}$ m^2/s; model equations, eqs 4.3 and 4.4; *k* values, Table 4.1.

closely the experimental points. Incorporation of H_2 limitation hardly improved the model predictions, and D_{H_2} could not be determined accurately. Figure 4.7 shows the plot of residuals. In contrast to hydrogenation of FAMEs, hydrogenation of oils appears to be affected by diffusion limitation of TAG rather than of H_2. Synthetic trioleate, diluted in saturated oil, was used as a check on the description of the *cis–trans* isomerization, because of the higher initial fraction of O and E, compared to partly hydrogenated sunflower oil. Figure 4.8 shows that the trioleate data can be described accurately by the model curves generated with the $D_{e,TAG}$ calculated from sunflower hydrogenations. So, the sunflower experiments series appear to provide TAG diffusion data relevant for synthetic trioleate as well.

We applied the FAME reaction mechanism and its intrinsic kinetic parameters for TAG hydrogenation, but there is some evidence that the catalyst activity in TAG hydrogenations may be 2-5 times lower than that of FAME (Van der Plank et al., 1972). However, the reduction in the kinetic parameters requires an increase in $D_{e,TAG}$ to fit the experimentally measured reaction flux, which also increases the catalyst efficiency to 1, thereby eliminating diffusion limitation.

In section 4.4.1 we have argued that in our reaction mechanism, only TAG or FAME diffusion limitation can account for a reduced production of *trans*. Therefore, the intrinsic kinetic rate parameters of FAME hydrogenation with TAG diffusion limitation form an unique combination to describe the observed significant reduction of trans in TAG hydrogenation.

4.4.4. Tracer Pulse Experiments: Test of Column Performance. Typical RTD curves of experimental runs are depicted in Figure 4.9, both for the RTD curves of the connecting lines only (inlet, outlet, detection cell) and for the whole system including the column, the latter curves situated at higher q. To obtain D_e with reasonable accuracy, the volume of inlet and outlet connectings were reduced to only 0.7% V_{cl} (column C2). The RTD curves of column + connecting lines were subsequently de-convoluted (Westerterp et al., 1987) with the appropriate (flow, tracer, temperature) RTD of the connecting lines. The two experimental series (C1 and C2, see Table 4.3) differ in eluent, but both columns are equally packed, using the same batch of particles. From Figure 4.9, it can be concluded that a uniform and regular packing was obtained.

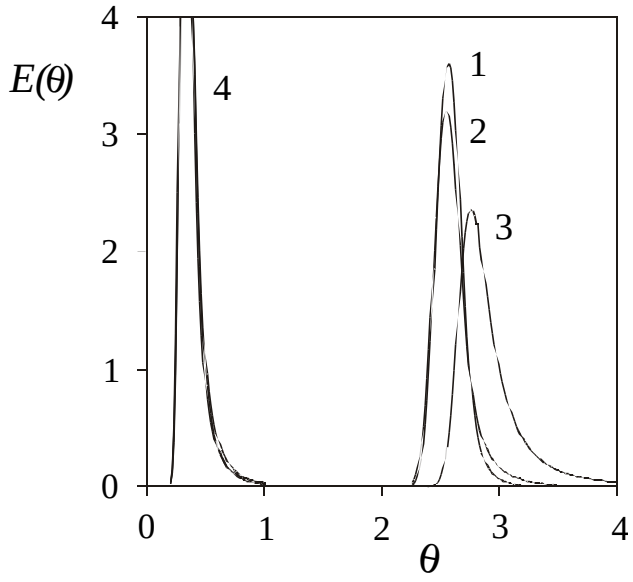

Figure 4.9. Residence time distribution curves for hexadecane and methyl palmitate (1), trioleate and soybean oil (2), cholesterol (3), and responses from connecting lines only (4) in medium-chain (carbon length, 10–12 atoms) triacylglyceride, T = 313 K. Column C2 (Table 4.3).

The bedporosity e_b was measured indirectly from both the column pressure drop according to Ergun's relation and from comparing RTD curves of adsorbing and non-

adsorbing tracers. For the laminar regime, Ergun's relation reads for spheres (Ergun, 1952):

$$\frac{\Delta P_{\mathrm{cl}}}{L} = 150 \frac{(1-e_{\mathrm{b}})^2}{e_{\mathrm{b}}^3} \frac{hu}{d_{\mathrm{p,S}}^2} \qquad (4.15)$$

Figure 4.10 shows that P_{cl}/hL for C1 and C2 coincide, though the viscosity of the eluents of C1 and C2 differed (0.45 and 17 mPa s respectively; the porosities of Ergun's relation of C1 (e_{b} = 0.26) and C2 (e_{b} = 0.28) proved to be identical).

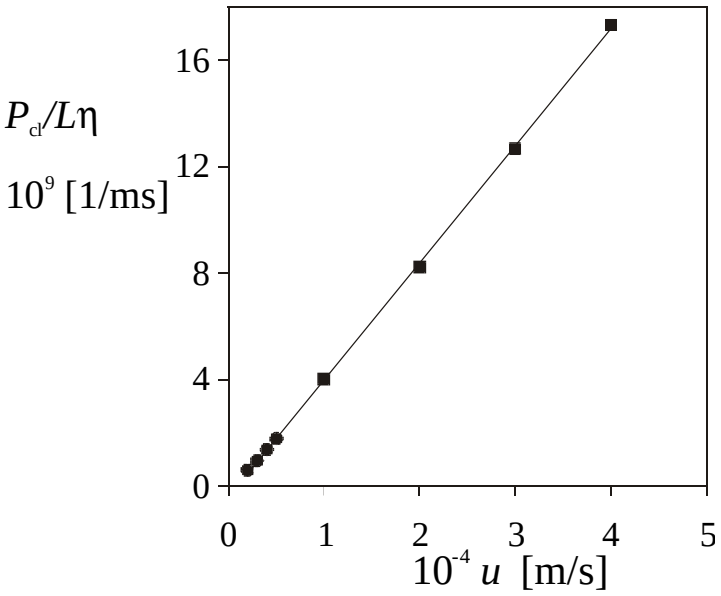

Figure 4.10. Pressure drop per meter per unit eluent viscosity, column C1 (♦) and C2 (●), as a function of the superficial velocity.

In absence of adsorption, the particle porosity, e_{p}, can be used as a check on e_{b}, because e_{p} is known from the manufacturer (e_{p} = 0.45). For column 1, RTD curves of TO and HD were found to be independent of temperature, so TO and HD are not subject to adsorption on the column packing ($K_{\mathrm{s}} \equiv 0$). Substituting e_{p} = 0.45 and K_{s} = 0 in eq 4.13, e_{b} can be calculated from the mean relative residence time, q_{m} (=MO1/t). Corrected for the response of the connecting lines, q_{m}(HD) = q_{m}(TO) = 2.25, e_{b} = 0.27, which is (practically) equal to the value obtained from Ergun's relation. Both from Ergun's relation and from the mean residence time, e_{b}'s around 0.27 were obtained,

which are not uncommon for micron-size particles with a Gaussian particle-size distribution (Cumberland and Crawford, 1987).

The parameters, V_r, Pe_{ax}, and D_e were simultaneously optimized from all the RTD curves of the tracers. Pe_{ax}/L could be obtained using all column peak responses simultaneously (Lin and Ma, 1989), while D_e and V_r are unique for each tracer. The input parameters were L, d_{cl}, Φ_v, and e_b and the experimental, deconvoluted tracer RTD. The fit procedure was as follows:

(1) The values of Pe_{ax}, V_r and D_e were separately fitted for all tracers in order to obtain starting values. A start value of V_r could also be obtained from eqs 4.13 and 4.14.

(2) All experimental series were simultaneously used to optimize Pe_{ax}, with the values of each series of V_r and D_e, of step 1.

(3) The V_r and the D_e of the tracers were optimised for the value of Pe_{ax} of step 2.

(4) Step 2 and 3 were repeated, until the values for V_r and D_e of the tracers and Pe_{ax} did not change anymore.

4.4.5. Intraparticle Diffusion under Nonreaction Conditions. The relation of Haynes and Sarma (1973) can be used to estimate the influence of the larger pores, compared to the smaller ones on the total mass transfer resistance. Using the moment method, Haynes and Sarma (1973) calculated for a bidisperse catalyst the contribution of the mass transfer in small pores relative to the large pore, denoted by a:

$$a = \frac{(1-e_{p,IH})e_{p,CR}^2(1+K_s)^2}{(e_{p,IH}+(1-e_{p,IH})e_{p,CR}(1+K_s))^2}\left(\frac{L_{p,CR}}{L_{p,IH}}\right)^2\left(\frac{D_{p,IH}}{D_{p,CR}}\right) \qquad (4.16)$$

In eq 4.16, $L_{p,CR}$ and $L_{p,IH}$ denote characteristic diffusion lengths in the crystallites and the intercrystalline holes, respectively. For both pore types, IH and CR, D_p is the pore diffusion coefficient, which is equal to the bulk diffusion coefficient, corrected for extra pore hindrance. e_p, is separated in a crystalline and intercrystalline voidage: $e_p = e_{p,CR} + e_{p,IH}$. The total particle void volume is defined by the BET isotherm, which is equal to the volume accessible to nitrogen, $V_{c,tot}$ = 0.17 mL/g, Figure 4.1A. The volume of the intercrystalline holes can be estimated from mercury porosimetry for the range of pores up to r_c = 0.5 *m*m, giving $V_{c,IH}$ = 0.05 mL/g (Figure 4.1B). Peaks above $r_c \approx 0.5$ *m*m arise from interparticle holes, due to particle settlement in the sample tube.

The total particle porosity is e_p = 0.45, which can now be divided in $e_{p,CR}$ = 0.31 and $e_{p,IH}$ = 0.14, for the crystalline pores and the intercrystalline holes, respectively. The characteristic length for the crystallites as estimated from Figure 4.2 is $L_{p,CR} \approx 0.5$ *m*m. The representative length of the inter crystalline holes is equal to the particle diameter, $L_{p,IH}$ = 10 *m*m.With $K_s < 0.2$ (from the experimental results), $1 + K_s \approx 1$, and $D_{p,CR} \approx 0.1 D_{p,IH}$ (conservative estimation), $a < 0.01$ is calculated from eq 4.16. Therefore, even for a relatively well-defined, small-pore-size range, the influence of the intracrystalline pores on the effective intraparticle diffusion coefficient is negligible.

Despite a relatively large particle size distribution (see Jonker et al., 1997), the obtained D_e can be regarded as representative for the batch of catalyst particles, because of the approximate Gaussian particle size distribution. Lin and Ma (1990) calculated that the use of an average particle size in obtaining D_e from pulse experiments appears to be a very good approximation, maybe because the slower mass transfer in the larger particles is compensated for by a faster mass transfer in the smaller particles (Lin and Ma, 1990).

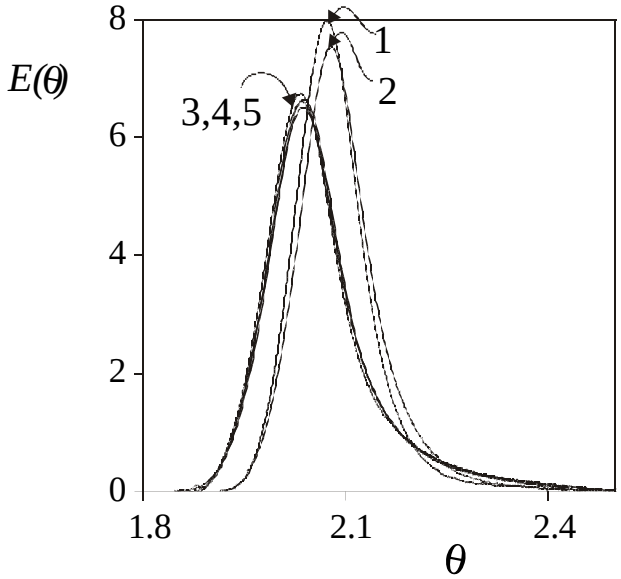

Figure 4.11. Residence time distribution curves for hexadecane (1), methyl palmitate (2), trioleate (3), and soybean oil (4) in MCT oil, T = 313 K. For trioleate, the curve at T = 300 K is also shown (5). Column C2 (Table 4.3).

With MCT oil as an eluent, typical experimental results and fits of TO and CH are shown in Figure 4.11 and Figure 4.12, respectively. The model curves agree very well with the nonadsorbing tracers (MP/HD/TO/SB), and showed some discrepancies in

case of CH, which can be ascribed to nonlinear adsorption (see the appendix of this chapter). The optimized values of V_r, D_e and Pe_{ax} are given in Table 4.7, including 95% confidence interval. The 95% confidence limit of D_e is obtained by calculations of c^2 boundaries (after Press et al., 1987). Due to the poor fit, the obtained D_e values of

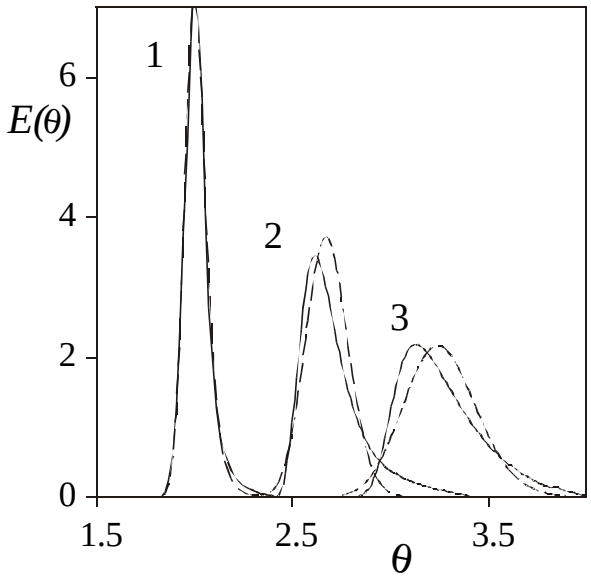

Figure 4.12. Experimental (solid line) and fitted curve (dashed line) residence time distribution curves for trioleate (1) and cholesterol: T = 353 K (2) and T = 313 K (3); column C2.

CH are only approximations. The value of $Pe_{ax} = 4.5 \times 10^3$ agrees nicely with the literature value $Bo = 0.5$ for an ideally packed column (Westerterp et al., 1987).

For *n*-octane the optimization was insensitive for D_e, because axial dispersion appeared to determine >97% of the dispersion effects, a commonly encountered phenomenon in tracer experiments (Haynes, 1988). Also, Hejtmánek and Schneider (1994) reported an almost negligible influence of a relatively large D_e, although 10-fold larger catalyst particles were applied. Pe_{ax} could be established at $(1.35 \pm 0.04) \times 10^3$, which leads to $Bo = 0.30 \pm 0.01$ (eq 4.12).

Table 4.7. D_e, Pe_{ax}, and V_r for Various Components in MCT oil[a]

tracer	T, K	$10^{11} D_e$, m^2/s	$10^{-3} Pe_{ax}$	$10^6 V_r$, m^3
methyl palmitate/*n*-hexadecane	313	$1.4 \le 1.7 \le 2.7$	4.5 ± 0.1	0.93 ± 0.01
trioleate/soy bean oil	313	$0.4 \le 0.5 \le 0.7$	4.5 ± 0.1	0.90 ± 0.01
cholesterol	313	≈ 0.02[b]	4.5 ± 0.1	1.39 ± 0.02
	353	≈ 0.05[b]	4.5 ± 0.1	1.20 ± 0.02

[a] Experimental data: see Table 4.1 (C2), $e_b = 0.28$. [b] confidence limits are less relevant, due to poor fit (Figure 4.12).

4.4.6. Comparison of D_e as measured by the different methods. The optimal D_{e,H_2} (1.6×10^{-10} m^2/s, T = 443 K) can be compared to the data of hydrogen diffusion in the bulk liquid phase only, because we are not aware of any literature data on the effective intraparticle diffusion coefficients of H_2, apart from Tsuto et al. (1978), who found for hydrogenation of methyl linoleate over a Pd/C catalyst $D_{e,H_2} = 3.6 \times 10^{-9}$ m^2/s, although the catalyst properties might be rather different. Andersson et al. (1974), and Ganguli and van den Berg (1978) determined $D_{b,H_2} = 2 \times 10^{-8}$ m^2/s (T = 443 K) for hydrogen diffusion in TAG mixtures. Applying the Wilke–Chang relation ($D_b \propto \sqrt{M_{solv}}/h_{solv}$, solv=solvent, TAG or FAME; Reid et al., 1987) suggests D_{b,H_2} in FAME to be a factor of 2 higher: D_{b,H_2} (FAME) $\approx 4 \times 10^{-8}$ m^2/s ($M_{FAME} = 0.33 M_{TAG}$, $h_{FAME} \approx 4 h_{TAG}$). Equation 4.1 suggests $D_{e,H_2} \approx 0.1 D_{b,H_2}$ ($e_p \approx 0.4$, $t \approx 4$, $l \approx 0$) yielding an estimated value of $D_{e,H_2} = 4 \times 10^{-9}$ m^2/s, which is in line with Tsuto et al. (1978). This values is above the upper confidence limit of our experimentally observed value ($D_{e,H_2} = 2.3 \times 10^{-10}$ m^2/s).

The temperature range for which $D_{e,TAG}$ was obtained (from the series of TAG experiments of Table 4.2) allows for a comparison with data on $D_{b,TAG}$ of Andersson et al. (1974), and Ganguli and van den Berg (1978). Andersson et al. (1974) showed the Stokes–Einstein relation (Dh/T = constant) to be applicable for the temperature dependency of liquid bulk diffusion coefficients. Equation 4.1 predicts $D_e(T) \propto D_b(T)$,

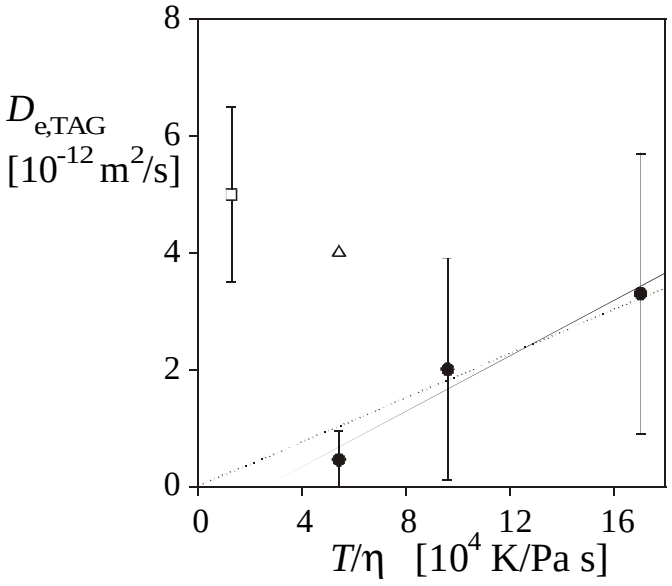

Figure 4.13. $D_{e,TAG}$ as f(T/h) for experiments 5–8 (Table 4.2), ● = $D_{e,TAG}$ from hydrogenation data (Pricat 9910, medium pore, $\langle d_c \rangle \approx 6$ nm), □ = $D_{e,TAG}$ from HPLC data (Pricat 9933, narrow pore, $\langle d_c \rangle \approx 4$ nm), Δ = $D_{e,TAG}$ from Colen et al. (1988) for medium-pore size hydrogenation catalyst. Solid line, regression of hydrogenation data; dotted line, the same but through the origin.

because e_b, t and l are temperature independent. Figure 4.13 shows D_e as a function of T/h for the hydrogenation data, with $h(T)$ from Wakeham and Magne (1946) and Eiteman and Goodrum (1994). Indeed, the dependency of D_e on T/h ($D_e h/T = 2 \times 10^{-7}$ (m^2Pa)/K) appears to be similar to that of D_b as reported by Andersson et al. (1974). The value of D_e from the hydrogenation experiments can also be related to the data of Colen et al. (1988), who performed hydrogenations at T = 373 K with trioleate, both with wide-pore and medium-pore catalysts. Their value of $D_{e,TAG} = 4 \times 10^{-12}$ m^2/s at T = 373 K for a medium-pore ($<d_c> \approx 6$ nm) catalyst is about 5 times higher, but still of the same order of magnitude as our value (see Figure 4.13). The observed value of $D_{e,TAG}$ from the HPLC experiments can be compared with $D_{e,TAG}$ calculated with equation 4.1 for wide pores. For large pores, t = 1.5 (Komiyama and Smith, 1974) and $l \rightarrow 0$, yielding (eq 4.1): $D_{e,IH} = 3 \times 10^{-12}$ m^2/s, which is rather close to the experimentally obtained value of 5×10^{-12} m^2/s, see Table 4.8. This is in line with Colen et al. (1988), who found for wide-pore catalysts, in which diffusion limitation was almost absent, a value of D_e of 5×10^{-12} m^2/s (extrapolated to T = 313 K). In contrast, the estimated value of $D_{e,CR}$ (for intercrystalline pores) is much smaller: taking an average value of t =3.5 (Leyva-Ramos and Geankoplis, 1994), $0.25 < l < 0.50$ (see Table 4.2), the range of $D_{e,CR}$ can be estimated as $3 \times 10^{-13} < D_{e,CR} < 1 \times 10^{-12}$ m^2/s. As the experimental value of $D_e = 5 \times 10^{-12}$ m^2/s is much larger, this confirms the dominating contribution of the larger pores.

Table 4.8. Comparison of Values of D_e

D_e calcd from	compound	λ	D_e(313K),m^2/s	source
HPLC	FAME	$\rightarrow 0$	$>10^{-11}$	this work
	TAG	0.25–0.50[a]	5×10^{-12}	this work
hydrogenations	TAG	0.25–0.50[a]	5×10^{-13}	this work
	TAG	0.3	1×10^{-12}	Colen et al., 1988
	TAG	$\rightarrow 0$	5×10^{-12}	Colen et al., 1988
estimation[b]	TAG	0.25–0.50[a]	$(0.3–1.0) \times 10^{-12}$	$\tau = 1.5$[c]
	TAG	$\rightarrow 0$	3×10^{-12}	$\tau = 3.5$[d]

[a] See Table 4.2. [b] With eq 4.1 and $D_{b,TAG} = 2.5 \times 10^{-12}$ m^2/s (Andersson et al., 1974), $e_p = 0.45$. [c] For large pores (Komiyama and Smith, 1974). [d] Average value (Leyva-Ramos and Geankoplis, 1994).

Comparison of $D_{e,TAG}$ (3.3×10^{-12} m^2/s, T = 443 K) obtained from TAG hydrogenations with experiments under inert conditions, ($4 \times 10^{-12} < D_e < 7 \times 10^{-12}$ m^2/s at T = 313 K) predicts, after extrapolation to T = 313 K, $D_{e,TAG}$(reaction) $\approx 0.1 D_{e,TAG}$(HPLC), see Figure 4.13. Also, McGreavy et al. (1994) and García-Ochoa

and Santos (1994) found a huge effect of the pore structure on D_e, whose influence varies with the experimental technique. D_e measured under inert conditions can be 2–20 times larger than D_e obtained from reaction data. They concluded that tracer techniques particularly give diffusivities in the macropores, resulting in diffusion coefficients up to 10 times larger, relative to diffusivities obtained from diffusion limited reaction data, depending on the pore structure. Although these effects were not completely understood, the latter, smaller, values are more relevant for describing diffusion-limited reaction, because the reaction proceeds in the micropores, where most of the active surface area is found.

4.5. Conclusions

FAME hydrogenations in Pricat 9910 (sample 1992) at T = 443 K, appear to be controlled by intraparticle diffusion of hydrogen. The intraparticle D_{e,H_2} could be calculated as $D_{e,H_2} = (1.6 \pm 0.6) \times 10^{-10}$ m^2/s at T = 443 K. As far as we know, this is the first result on intraparticle hydrogen diffusion in FAME hydrogenation on supported nickel catalysts. In TAG hydrogenation, both at 373 K and 443 K, TAG appears to be diffusion limited ($D_{e,TAG} = (3.3 \pm 1.1) \times 10^{-12}$ m^2/s, T = 443 K), rather than H_2, which is in line with literature.

Intraparticle pore diffusion was measured for paraffins, triacylglycerides and methyl esters of fatty acids in Pricat 9933 by a so-called HPLC tracer technique. Because of the small particles and relatively fast intraparticle mass transfer, these experiments are unique in the literature. The response peaks indicate a uniform packing of the particles over the column, without bypasses or dead zones, which was confirmed by consistent bed voidages ($\varepsilon_b = 0.27 \pm 0.01$), and Peclet numbers for axial dispersion of 0.5, which is the value expected for ideally packed columns. Intraparticle diffusivities of methyl palmitate and *n*-hexadecane in MCT oil were measured as $1.4 \times 10^{-11} < D_e < 2.7 \times 10^{-11}$ m^2/s in *n*-octane (95% confidence limit, T = 313 K). For trioleate and soybean oil $4 \times 10^{-12} < D_e < 7 \times 10^{-12}$ m^2/s was observed.

The relatively large value of D_e in HPLC experiments indicate a small hindrance in the pores, which can be ascribed to a large influence of intercrystalline holes, relative to the crystalline pores. The observed $D_{e,TAG}$ under reaction conditions appeared to be 10-fold lower than measured with a tracer technique under nonreaction conditions. This difference could be qualitatively explained from the fact that tracer techniques measure the diffusivity in the macropores, whereas the chemical reaction mostly occurs in micropores.

Appendix: Nonequilibrium Adsorption

The cholesterol RTD curves show back tailing, which may indicate nonlinear adsorption (Ruthven, 1984). However, nonlinear adsorption necessarily leads to a dependency of the elution pattern on the concentration of injected tracer (Ma and Lin, 1990), which is in contrast with our findings. Back tailing can also be caused by an extra kinetic effect, as nonequilibrium adsorption (Giddings, 1963). A molecule is then assumed to adsorb on two different sites, with and without the extra kinetic effect respectively, with a chance calculated with a probability function (Giddings and Eyring, 1955; Giddings, 1963). The use of the probabilities enables the numerical addition of an extra kinetic effect on the column dispersion.

Giddings (1963) demonstrated that tailing can have a kinetic background, such as a nonequilibrium adsorption–desorption processes, which is superimposed on the dispersion effects. Two kind of sites are assumed in the column packing: apart from the "normal" sites with equilibrium adsorption, a category of independently operating sites are added, on which an extra kinetic effect occurs. The extra kinetic effect is modeled as a first-order forward rate and a first-order backward rate, without further specification, although it can be seen as nonequilibrium adsorption. The probability of a molecule adsorbing at the equilibrium sites, $P'(y)$ is equal to:

$$P'(y) = e^{-k_f t_m} d(y) \qquad (4.A1)$$

with k_f the first order (forward) kinetic constant on the nonequilibrium sites (s^{-1}) and $\delta(y)$ the input (Dirac) response pulse. The y is defined as t_s/t_m, with t_m the mean residence time and t_s the (variable) time spent adsorbed on the tail-producing site which is thus the time measured from the appearance of a normal peak-i.e., a peak undisturbed by the extra kinetic effect. The probability of the molecule adsorbing on the non-linear part is described by the Poisson-distribution, which leads to (Giddings and Eyring, 1955; Giddings, 1963)

$$P(y) = \left(\frac{k_f k_b}{y}\right)^{0.5} e^{-(k_f + k_b y) t_m} I_1\left(\sqrt{4 k_f k_b t_m^2 y}\right) \qquad (4.A2)$$

with k_b (backwards) first-order kinetic rate constant for desorption from the nonequilibrium sites (s^{-1}). The I_1 is the first order Bessel function of imaginary argument. By definition, *P(y)* and *P'(y)* count up to one. Because eqs 4.A1 and 4.A2 represent a probability distribution, the dispersion effects of axial and intraparticle mass transfer can be treated as separate and serial processes (Giddings, 1963). The peak dispersion of the column is therefore convoluted with eq 4.A1 and eq 4.A2. The resulting response curves contain subsequently the influence of an extra, nonequilibrium effect.

Figure 4.A1 shows the curves *P(y)* and *P'(y)*, which account for the adsorption on equilibrium adsorption sites and on nonequilibrium sites, respectively. Both curves are corrected for dispersion effects and influences of the connecting lines. The summation of *P(y)* and *P'(y)* fairly better describes the experimental RTD than eq 4.6 alone. The better fit results in a more accurate value of D_e than the fit of Figure 4.12: $D_{e,CH} = 0.63 \times 10^{-12}$ and 2.2×10^{12} m^2/s for T = 313 and 353 K respectively. The fit values of k_f and k_b are strongly dependent on the start values, which implies that the CH curves contain too less information to obtain reliable values for k_f and k_b. As Giddings (1963) already stated, nonequilibrium adsorption curves may in some cases better explain severe back tailing of RTD curves, instead of the more commonly applied nonlinear adsorption.

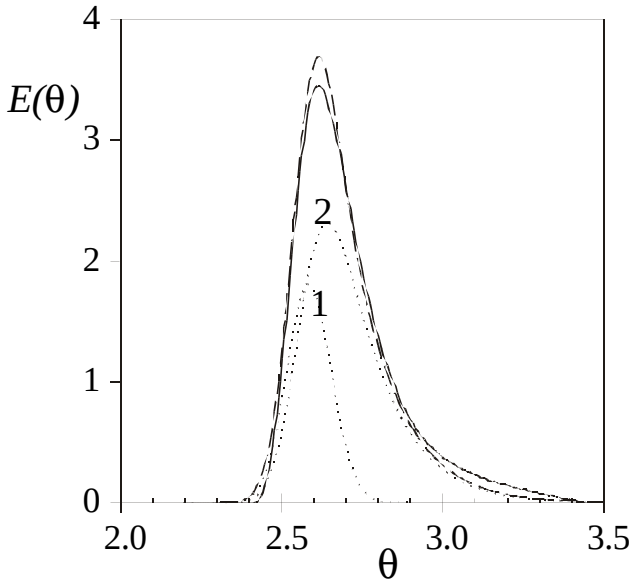

Figure 4.A1. Fit of residence time distribution curve of cholesterol (T = 353 K). Solid line: experiment; dotted line '1': contribution of equilibrium adsorption; dotted line '2': contribution of nonequilibrium adsorption; dashed line: summation of dotted line '1' and '2'.